J|A|C|S ARTICLES

Published on Web 10/21/2010

Synthesis and Magnetic Properties of Gd Doped EuS Nanocrystals with Enhanced Curie Temperatures

Rachel S. Selinsky, Jae Hyo Han, Elvin A. Morales Pérez, Ilia A. Guzei, and Song Jin*

Department of Chemistry, University of Wisconsin—Madison, 1101 University Avenue, Madison, Wisconsin 53706, United States

Received May 18, 2010; E-mail: jin@chem.wisc.edu

Abstract: EuS nanocrystals (NCs) were doped with Gd resulting in an enhancement of their magnetic properties. New EuS and GdS single source precursors (SSPs) were synthesized, characterized, and employed to synthesize $Eu_{1-x}Gd_xS$ NCs by decomposition in oleylamine and trioctylphosphine at 290 °C. The doped NCs were characterized using X-ray diffraction, transmission electron microscopy, and scanning transmission electron microscopy, which support the uniform distribution of Gd dopants through electron energy loss spectroscopy (EELS) mapping. X-ray absorption spectroscopy (XAS) revealed the dopant ions in $Eu_{1-x}Gd_xS$ NCs to be predominantly Gd^{3+}. NCs with a variety of doping ratios of Gd ($0 \leq x < 1$) were systematically studied using vibrating sample magnetometry and the observed magnetic properties were correlated with the Gd doping levels (x) as quantified with ICP-AES. Enhancement of the Curie temperature (T_C) was observed for samples with low Gd concentrations ($x \leq 10\%$) with a maximum T_C of 29.4 K observed for NCs containing 5.3% Gd. Overall, the observed T_C, Weiss temperature (θ), and hysteretic behavior correspond directly to the doping level in $Eu_{1-x}Gd_xS$ NCs and the trends qualitatively follow those previously reported for bulk and thin film samples.

Introduction

Magnetic semiconductors, materials whose magnetic and electronic properties are coupled, hold promise for applications in spintronics and magneto-optics.[1−6] To harness these physical capabilities, there has been significant study into many compositions and morphologies of such materials, most recently focusing on nanostructures.[6−12] An extensively studied subset of model magnetic semiconductors are the europium chalcogenides (EuQ, where Q = O, S, Se, Te), whose magnetic behavior ranges from ferromagnetic EuS and EuO to antiferromagnetic EuTe.[6,13−15] As a concentrated ferromagnetic semiconductor (band gap 1.6 eV) in which the aligned magnetic spins are intrinsic to the lattice, EuS is an appealing material.[16−19] Furthermore, EuS has a high spin polarization (86%), a large band splitting (0.36 eV when $T < T_C$), and large effective magnetic moment (7.9 μ_B).[13,14] Despite these promising characteristics, its low Curie temperature (T_C, the temperature at which it transitions from paramagnetic to ferromagnetic behavior) of 16.6 K makes it impractical for device applications without enhancement.

As a well-understood intrinsic ferromagnetic semiconductor, EuS is a model material for exploring modulation of magnetism in nanocrystals (NCs). Magnetic semiconductors can benefit from being synthesized and studied on the nanoscale. The high surface to volume ratio of NCs means that the surface activity has an increased contribution to the overall behavior of the material as compared to the bulk, so modification to the surface can allow for modulation of electronic and magnetic properties.[9,20] When the crystals' size is small enough that the anisotropy energy of the NC is comparable to the thermal energy, they begin to exhibit superparamagnetic behavior.[21−27] Solution

(1) Felser, C.; Fecher, G. H.; Balke, B. *Angew. Chem., Int. Ed.* **2007**, *46*, 668.
(2) Ando, K. *Science* **2006**, *312*, 1883.
(3) Wolf, S. A.; Awschalom, D. D.; Buhrman, R. A.; Daughton, J. M.; Von Molnar, S.; Roukes, M. L.; Chtchelkanova, A. Y.; Treger, D. M. *Science* **2001**, *294*, 1488.
(4) Ohno, Y.; Young, D. K.; Beschoten, B.; Matsukura, F.; Ohno, H.; Awschalom, D. D. *Nature* **1999**, *402*, 790.
(5) Zutic, I.; Fabian, J.; Das Sarma, S. *Rev. Mod. Phys.* **2004**, *76*, 323.
(6) Bierman, M. J.; Van Heuvelen, K. M.; Schmeisser, D.; Brunold, T. C.; Jin, S. *Adv. Mater.* **2007**, *19*, 2677.
(7) Beaulac, R.; Archer, P. I.; Ochsenbein, S. T.; Gamelin, D. R. *Adv. Funct. Mater.* **2008**, *18*, 3873.
(8) Kulkarni, J. S.; Kazakova, O.; Holmes, J. D. *Appl. Phys. A: Mater. Sci. Process.* **2006**, *85*, 277.
(9) Lu, A. H.; Salabas, E. L.; Schuth, F. *Angew. Chem., Int. Ed.* **2007**, *46*, 1222.
(10) LesliePelecky, D. L.; Rieke, R. D. *Chem. Mater.* **1996**, *8*, 1770.
(11) Song, Y.; Schmitt, A. L.; Jin, S. *Nano Lett.* **2008**, *8*, 2356.
(12) Schmitt, A. L.; Higgins, J. M.; Jin, S. *Nano Lett.* **2008**, *8*, 810.
(13) Mauger, A.; Godart, C. *Phys. Rep.* **1986**, *141*, 51.
(14) Wachter, P. *Europium Chalcogenides: EuO, EuS, EuSe and EuTe*; North-Holland: Amsterdam, 1979; Vol. 2.
(15) Suits, J. C.; Argyle, B. E.; Freiser, M. J. *J. Appl. Phys.* **1966**, *37*, 1391.
(16) Von Molnar, S.; Read, D. *Proc. IEEE* **2003**, *91*, 715.
(17) Filip, A. T.; LeClair, P.; Smits, C. J. P.; Kohlhepp, J. T.; Swagten, H. J. M.; Koopmans, B.; de Jonge, W. J. M. *Appl. Phys. Lett.* **2002**, *81*, 1815.
(18) Ren, C.; Trbovic, J.; Kallaher, R. L.; Braden, J. G.; Parker, J. S.; von Molnar, S.; Xiong, P. *Phys. Rev. B* **2007**, *75*.
(19) Ren, C.; Trbovic, J.; Xiong, P.; von Molnar, S. *Appl. Phys. Lett.* **2005**, *86*, 012501.
(20) Alivisatos, A. P. *Science* **1996**, *271*, 933.
(21) Hyeon, T. *Chem. Commun.* **2003**, *927*.
(22) Sun, S. H. *Adv. Mater.* **2006**, *18*, 393.
(23) McHenry, M. E.; Willard, M. A.; Laughlin, D. E. *Prog. Mater Sci.* **1999**, *44*, 291.

synthesis of NCs enables large quantities of material to be prepared and allows for improved processing and assembly; for instance, EuS NCs can be employed as starting materials for the synthesis of magnetic composites.[28−34]

Utilization of magnetic semiconductors such as EuS for practical applications depends on the ability to improve and/or tailor their electronic and magnetic properties. In the case of EuS NCs, a major obstacle is the low T_C; therefore, developing a method for enhancing the T_C is crucial. Doping with Gd to form $Eu_{1-x}Gd_xS$ in bulk and thin film samples has been shown to enhance the T_C to ∼50 K. The similar lattice parameters of the same rock salt structure types (5.968 Å for EuS as compared to 5.5655 Å for GdS) and similar ionic radii (1.15 Å for Eu^{2+} as compared to 1.12 Å for Gd^{2+} and 0.938 Å for Gd^{3+}) allow for exchange of Eu ions with Gd ions to create doped crystals for all ratios of Eu and Gd.[35,36] EuS is an ideal Heisenberg ferromagnet where each Eu^{2+} ion carries the full magnetic moment of all unpaired spins of half-filled 4f shell.[13,14] GdS itself is an antiferromagnetic metal with a Néel temperature (T_N) of 59 K.[37] Doping EuS with trivalent Gd ions, which also have the $4f^7$ spin ground state, introduces additional electrons without significantly impacting the spin structure. These additional electrons first compensate for the Eu^{3+} acceptor states known to be common defects in EuS, then a small number of additional electrons significantly increase both T_C and θ (the Weiss constant) at low Gd doping level ($x < 0.2$). Such enhancement peaks for $0.01 \leq x \leq 0.03$ in the bulk, because this enhancement of magnetic coupling is due to an oscillatory RKKY-type indirect exchange mechanism: when the doping level is further increased, magnetic benefits rapidly decrease, resulting in loss of enhancement and ultimately the emergence of antiferromagnetic behavior, like that seen in GdS.[14,38−40]

Although methods for preparing bulk $Eu_{1-x}Gd_xS$ have been developed including co-melting and cooling of EuS and GdS ingots, electron-beam deposition, and flash evaporation,[39,41] Gd doping of EuS NCs has not been previously reported. Pure EuS NCs can be synthesized using a variety of methods including growth from liquid ammonia,[42,43] white light[44] and microwave irradiation,[45] zeolite templating,[46] and decomposition of single source precursors.[47,48] The traditional colloidal syntheses using separate precursors that are more prevalent for common NC growth have not been shown to be effective for synthesizing EuS NCs. Synthesis through decomposition of single source precursors (SSPs) of europium complexes with dithiocarbamate (dtc) ligands have yielded good quality, monodisperse, single crystalline EuS NCs with a stable coating of organic capping ligands.[26,34,47−54]

Scheme 1. Chemical Structures and Abbreviations for the Ligands in $Eu(Dtc)_3L$ and $Gd(Dtc)_3L$[a]

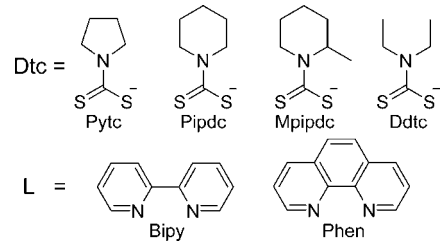

[a] The precursors as seen in Table 1 are as follows: $Eu(Pytc)_3Bipy$ (**1**), $Eu(Pipdc)_3Bipy$ (**2**), $Eu(Mpipdc)_3Phen$ (**3**), $Gd(Pytc)_3Bipy$ (**4**), $Gd(Ddtc)_3$-Bipy (**5**).

In this work, in order to improve the EuS NC synthesis and enable effective doping, we first expanded the repertoire of SSPs by synthesizing and characterizing three new Eu dtc SSPs and two new Gd dtc SSPs using the ligand library shown in Scheme 1. We tested each precursor using a set of standard reaction conditions and focused on one EuS SSP, $Eu(Pytc)_3Bipy$ (**1**) and its structurally similar Gd SSP, $Gd(Pytc)_3Bipy$ (**4**) due to somewhat improved morphology and crystallinity. We then developed the methods for reproducibly synthesizing $Eu_{1-x}Gd_xS$ NCs with a range of doping ratios (x) using the simultaneous decomposition of mixtures of Eu and Gd SSPs **1** and **4**. Finally, systematic structural and magnetic characterization of this series of doped NCs will be presented to show the effect of Gd incorporation on the enhancement of Curie temperatures and magnetic properties of EuS NCs.

Experimental Section

Pipecolyldithiocarbamic acid pipecolinium salt was purchased from TCI America. All other chemicals were purchased from Sigma-Aldrich Chemical Co. They were used without further purification unless otherwise noted. For syntheses of $Eu(Pytc)_3Bipy$,

(24) Bucher, J. P.; Douglass, D. C.; Bloomfield, L. A. *Phys. Rev. Lett.* **1991**, *66*, 3052.
(25) Billas, I. M. L.; Chatelain, A.; Deheer, W. A. *Science* **1994**, *265*, 1682.
(26) Regulacio, M. D.; Kar, S.; Zuniga, E.; Wang, G.; Dollahon, N. R.; Yee, G. T.; Stoll, S. L. *Chem. Mater.* **2008**, *20*, 3368.
(27) Redígolo, M. L.; Koktysh, D. S.; van Benthem, K.; Rosenthal, S. J.; Dickerson, J. H. *Mater. Chem. Phys.* **2009**, *115*, 526.
(28) Zeng, H.; Li, J.; Liu, J. P.; Wang, Z. L.; Sun, S. H. *Nature* **2002**, *420*, 395.
(29) Sun, S. H.; Murray, C. B.; Weller, D.; Folks, L.; Moser, A. *Science* **2000**, *287*, 1989.
(30) Fullerton, E. E.; Jiang, J. S.; Bader, S. D. *J. Magn. Magn. Mater.* **1999**, *200*, 392.
(31) Hadjipanayis, G. C. *J. Magn. Magn. Mater.* **1999**, *200*, 373.
(32) Fumagalli, P.; Schirmeisen, A.; Gambino, R. J. *Phys. Rev. B* **1998**, *57*, 14294.
(33) Tang, J.; O'Connor, C. E.; Feng, L. *J. Alloys Compd.* **1998**, *275*, 606.
(34) Tanaka, A.; Kamikubo, H.; Doi, Y.; Hinatsu, Y.; Kataoka, M.; Kawai, T.; Hasegawa, Y. *Chem. Mater.* **2010**, *22*, 1776.
(35) Templeton, D. H.; Dauben, C. H. *J. Am. Chem. Soc.* **1954**, *76*, 5237.
(36) Wachter, P. *Phys. Rep.* **1978**, *44*, 159.
(37) Brückel, T.; Hupfeld, D.; Strempfer, J.; Caliebe, W.; Mattenberger, K.; Stunault, A.; Bernhoeft, N.; McIntyre, G. J. *Eur. Phys. J. B* **2001**, *19*, 475.
(38) Kasuya, T. *IBM J. Res. Dev.* **1970**, *14*, 214.
(39) McGuire, T. R.; Holtzberg, F. *AIP Conf. Proc.* **1972**, *5*, 855.
(40) Holtzberg, F.; McGuire, T. R.; Methfessel, S.; Suits, J. C. *Phys. Rev. Lett.* **1964**, *13*, 18.
(41) Bayer, E.; Zinn, W. *IEEE Trans. Magn.* **1973**, *MAG9*, 4.
(42) Thongchant, S.; Hasegawa, Y.; Wada, Y.; Yanagida, S. *Chem. Lett.* **2003**, *32*, 706.
(43) Thongchant, S.; Hasegawa, Y.; Wada, Y.; Yanagida, S. *J. Phys. Chem. B* **2003**, *107*, 2193.
(44) Hasegawa, Y.; Afzaal, M.; O'Brien, P.; Wada, Y.; Yanagida, S. *Chem. Commun.* **2005**, *242*.
(45) Hasegawa, Y.; Okada, Y.; Kataoka, T.; Sakata, T.; Mori, H.; Wada, Y. *J. Phys. Chem. B* **2006**, *110*, 9008.
(46) Chen, W.; Zhang, X. H.; Huang, Y. N. *Appl. Phys. Lett.* **2000**, *76*, 2328.
(47) Regulacio, M. D.; Tomson, N.; Stoll, S. L. *Chem. Mater.* **2005**, *17*, 3114.
(48) Mirkovic, T.; Hines, M. A.; Nair, P. S.; Scholes, G. D. *Chem. Mater.* **2005**, *17*, 3451.
(49) Zhao, F.; Sun, H. L.; Gao, S.; Su, G. *J. Mater. Chem.* **2005**, *15*, 4209.
(50) Redigolo, M. L.; Koktysh, D. S.; Rosenthal, S. J.; Dickerson, J. H.; Gai, Z.; Gao, L.; Shen, J. *Appl. Phys. Lett.* **2006**, *89*.
(51) Zhao, F.; Sun, H. L.; Su, G.; Gao, S. *Small* **2006**, *2*, 244.
(52) Regulacio, M. D.; Bussmann, K.; Lewis, B.; Stoll, S. L. *J. Am. Chem. Soc.* **2006**, *128*, 11173.
(53) Huxter, V. M.; Mirkovic, T.; Nair, P. S.; Scholes, G. D. *Adv. Mater.* **2008**, *20*, 2439.
(54) Pereira, A. S.; Rauwel, P.; Reis, M. S.; Silva, N. J. O.; Barros-Timmons, A.; Trindade, T. *J. Mater. Chem.* **2008**, *18*, 4572.

Table 1. Summary of Crystal Data Structure Refinement for $Eu(Dtc)_3L$ and $Gd(Dtc)_3bipy$

	(**1**) $Eu(Pytc)_3Bipy$	(**2**) $Eu(Pipdc)_3Bipy$	(**3**) $Eu(Mpipdc)_3Phen$	(**4**) $Gd(Pytc)_3Bipy$	(**5**) $Gd(Ddtc)_3Bipy$
Empirical Formula	$EuC_{25}H_{32}N_5S_6 \cdot 3CHCl_3$	$EuC_{28}H_{38}N_5S_6 \cdot CHCl_3$	$EuC_{33}H_{47}N_5S_6 \cdot 3CHCl_3$	$GdC_{25}H_{32}N_5S_6 \cdot 3CHCl_3$	$GdC_{25}H_{38}N_5S_6$
Formula Weight	1104.98	908.32	1213.16	1110.27	758.21
Crystals system	Orthorhombic	Monoclinic	Triclinic	Orthorhombic	Monoclinic
Space group	*Pbca*	$P2_1/c$	$P\bar{1}$	*Pbca*	$P2_1/c$
a (Å)	18.2696(16)	17.4375(5)	10.9505(3)	18.2665(13)	17.3870(4)
b (Å)	17.3678(15)	15.3706(4)	13.0006(4)	17.3854(12)	10.5216(2)
c (Å)	26.635(2)	13.7483(3)	18.4281(5)	26.6725(19)	17.2950(4)
α (deg)	90	90	99.158(2)	90	90
β (deg)	90	92.703(2)	95.478(2)	90	96.6080(10)
γ (deg)	90	90	103.997(2)	90	90
Volume ($Å^3$)	8451.4(13)	3680.79(16)	2488.44(12)	8470.4(10)	3142.91(12)
Z	8	4	2	8	4
Wavelength (Å)	0.71073	1.54178	1.54178	0.71073	1.54178
Density (calc) (mg/m^3)	1.737	1.639	1.619	1.741	1.602
Abs Coefficient (mm^{-1})	2.379	17.609	16.083	2.459	17.558
Crystal size (mm^3)	0.32 × 0.23 × 0.16	0.47 × 0.40 × 0.08	0.30 × 0.12 × 0.08	0.50 × 0.50 × 0.20	0.32 × 0.30 × 0.28
θ range (deg)	2.23−28.70	2.54−71.22	2.45−71.64	1.79−30.00	4.92−71.83
Reflections Collected	116495	39811	41777	151308	49621
Independent Reflections	10905(0.0760)	6860(0.0621)	9452(0.0469)	12320(0.0333)	5949(0.0335)
Data/Restraints/Parameters	10905/0/442	6860/0/397	9152/1270	12320/0/442	5949/0/340
GOF on F^2	0.962	1.058	1.016	0.947	1.076
R_1/wR_2 [$I > 2\sigma$]	0.0363/0.0903	0.0511/0.1232	0.0544/0.1419	0.0264/0.0642	0.0227/0.0587

$Gd(Pytc)_3Bipy$, and $Gd(Ddtc)_3Bipy$, the dithiocarbamate salts were recrystallized from hot ethanol prior to use.

Synthesis of NH_4·Pipdc. As piperidine dithiocarbamate is not available commercially, it was prepared following a standard procedure. To an ice bath containing a flask with a vigorously stirring mixture of mixture of 0.5 mol 35% NH_4OH (1.97 mL, 0.88 g/mL) in 15 mL of 1:1 (v/v) ethanol/H_2O was added 0.05 mol (4.94 mL) of piperidine. Carbon disulfide 0.05 mol (3.02 mL) was slowly added dropwise resulting in the precipitation of the dithiocarbamate salt. After the resultant yellow mixture was stirred for 30 min, white crystals were collected by vacuum filtration, washed with cold ethanol, and dried under vacuum.

Synthesis of $Eu(Pytc)_3Bipy$ (1), $Eu(Pipdc)_3Bipy$ (2), and $Eu(Mpipdc)_3Phen$ (3). Europium pyrrolidine dithiocarbamate, $Eu(Pytc)_3Bipy$ (**1**); piperidine dithiocarbamate bipyridine, $Eu(Pipdc)_3$-Bipy (**2**); and europium pipecolyl dithiocarbamate phenanthroline, $Eu(Mpipdc)_3Phen$ (**3**) were prepared based on previously published procedures.[47−49] A clear solution of 1 mmol (0.366 g) of $EuCl_3 \cdot 6H_2O$ in 10 mL boiling distilled water was added dropwise to a clear solution of 1 mmol (0.156 g) of 2,2′-bipyridine or 1 mmol (0.180 g) of 1,10-phenanthroline in 10 mL of boiling distilled water. A clear solution of 3 mmol of the desired dithiocarbamate salt in 30 mL of dH_2O was prepared (0.492 g of NH_4·Pytc for **1**; 0.523 g of NH_4·Pipdc for **2**; or 0.823 g of Mpipdc for **3**). The dithiocarbamate solutions were then added dropwise to the vigorously stirred solution of europium salt and 2,2′-bipyridine or 1,10′-phenanthroline, rapidly forming crystals of the respective SSP (orange for **1**, red-orange for **2**, and red-orange for **3**). After stirring for 20 min and then cooling in an ice bath, the crystals were collected by vacuum filtration, rinsed with cold dH_2O, and stored in a desiccator in the dark. The yield was ∼64% for **1**, ∼30% for **2**, and <20% for **3**. IR for **1** $\nu_{C-N} = 1473\ cm^{-1}$, $\nu_{C-S} = 1012\ cm^{-1}$; **2** $\nu_{C-N} = 1477\ cm^{-1}$, $\nu_{C-S} = 1012\ cm^{-1}$; **3** $\nu_{C-N} = 1468\ cm^{-1}$, $\nu_{C-S} = 1002\ cm^{-1}$.

Synthesis of $Gd(Pytc)_3Bipy$ (4) and $Gd(Ddtc)_3Bipy$ (5). The procedure for preparing the Gd SSPs was slightly modified from that for Eu SSPs. To a 10 mL solution of 1 mmol (0.327 g) of $Gd(NO_3)_3 \cdot 6H_2O$ was added a solution of 2,2′-bipyridine (1 mmol, 0.156 g) in 10 mL of boiling dH_2O. The dithiocarbamate salts used were NH_4·Pytc and Na·Ddtc (3 mmol, 0.492 and 0.514 g, respectively). Upon addition of the dithiocarbamate salts to the lanthanide and bipyridine mixture, off-white crystals were rapidly formed. After stirring for 20 min and cooling in an ice bath, the crystals were collected by vacuum filtration, rinsed with cold dH_2O, and stored in a desiccator in the dark. The yield was ∼68 for **4** and ∼46% for **5**. IR for **4** $\nu_{C-N} = 1473\ cm^{-1}$, $\nu_{C-S} = 1012\ cm^{-1}$; **5** $\nu_{C-N} = 1482\ cm^{-1}$, $\nu_{C-S} = 1006\ cm^{-1}$.

Characterization of the SSPs. The precursors were characterized by FTIR, single-crystal X-ray crystallography, and thermogravimetric analysis. SSPs dissolved in chloroform were dropcast onto ZnSe windows and IR spectra were taken using a Nicolet 740 FTIR from 800 and 4000 cm^{-1}. Alternatively, dry, powdered samples were observed using an attenuated total reflectance (ATR) attachment on a Nicolet 740 FTIR. Thermogravimetric analysis was performed on a Netzsch STA 409CD thermogravametric analyzer in a Pt pan from 100 to 650 °C under flowing N_2 gas. Single crystals for X-ray crystallographic analysis were grown by slowly diffusing isopropyl alcohol or hexanes into $CHCl_3$ solutions of SSPs. The data collection parameters and refinement results are presented in Table 1. Full details of crystal structure determination are included in the Supporting Information.

Synthesis of $Eu_{1-x}Gd_xS$ NCs. All SSPs were made fresh within 2 weeks before NC synthesis. The procedure for synthesizing the doped $Eu_{1-x}Gd_xS$ NCs was modified from published procedures[47−51] for synthesizing EuS NCs but using SSPs **1** and **4**. The desired molar ratio of Eu to Gd SSPs was determined such that the molar sum of both SSPs was 0.1125 mmol. For example, to synthesize EuS NCs ($x = 0$), 0.1125 mmol (0.0840 g) of $Eu(Pytc)_3Bipy$ (**1**) was required; to synthesize $Eu_{0.5}Gd_{0.5}S$ ($x = 0.5$), 0.563 mmol (0.0420 g) of **1** and 0.563 mmol (0.0423 g) **4** were required. The precursors were suspended in 2 mL of trioctylphosphine (TOP) and degassed under vacuum for 30 min. In a three-necked flask outfitted with a septum and a thermocouple, 3 mL of oleylamine was kept at 120 °C under vacuum for 30 min, then heated to 290 °C under N_2, after which the precursor suspension was rapidly injected into the solution under vigorous stirring. After 30 min of stirring at 290 °C, 15 mL of anhydrous ethanol was injected and the solution was centrifuged for 30 min at 3500 rpm giving a dark purple precipitate and a pale yellow supernatant which was discarded. The precipitate was resuspended in 2 mL of ethyl acetate, precipitated with 40 mL of ethanol, and centrifuged for 30 min at 3500 rpm. The solid was dried under a stream of nitrogen and stored under inert atmosphere in a glovebox. The products varied in color from dark purple for pure EuS NCs to brown for pure GdS NCs.

Characterization of $Eu_{1-x}Gd_xS$ NCs. The structure and composition of $Eu_{1-x}Gd_xS$ NCs were characterized by transmission electron microscopy (TEM), scanning transmission electron microscopy (STEM), powder X-ray diffraction (PXRD), and ion-coupled plasma atomic emission spectroscopy (ICP-AES). $Eu_{1-x}Gd_xS$ NCs suspended in chloroform were dropcast onto TEM

grids with lacey carbon films for STEM and TEM analysis. HRTEM imaging was performed on a Phillips CMT200 TEM with an accelerating voltage of 200 kV. STEM results were obtained on a 200 kV FEI Titan STEM with CEOS hexapole aberration corrector. Noise in the EELS spectrum image was reduced using principle component analysis (PCA), retaining the first 6 principal components.[55] Samples for PXRD were prepared by dropcasting $Eu_{1-x}Gd_xS$ NCs from a chloroform suspension onto Si substrates. PXRD was collected on a Siemens STOE diffractometer using Cu Kα radiation.

Knowing the exact ratio of Gd to Eu in each $Eu_{1-x}Gd_xS$ NC sample is crucial to this study. To determine these ratios, ICP-AES was performed using a Perkin-Elmer Optima 2000 DV Optical Emission Spectrometer. ICP-AES samples were prepared by thoroughly drying the $Eu_{1-x}Gd_xS$ NCs to a powder, then digesting the NCs to ions with concentrated (68%) HNO_3 and diluting to 5% HNO_3. Calibration standards were made by diluting 1000 ppm standards of both Eu and Gd (purchased from GFS chemicals) over the range of 0.5−3.2 ppm for each. Calibration curves for high and low concentrations were made for three emission wavelengths because instrument response was not linear over the broad range of concentrations required to accurately determine small x values. Three emission wavelengths for each Eu (381.967, 393.048, and 412.97 nm) and Gd (336.223, 342.247, and 376.839 nm) were measured. Concentrations were calculated from the emission intensities for the three Gd and three Eu wavelengths for each sample were converted to concentrations using the appropriate calibration curves and averaged.

X-ray Absorption Spectroscopy. Synchrotron X-ray Absorption Spectroscopy (XAS) measurements were performed at the Advanced Photon Source at Argonne National Laboratory using beamline 4-ID-C. The NCs were dropcast onto silicon substrates and were placed in a split-coil superconducting solenoid in a liquid He cryostat. X-rays absorption scans were performed at 8 K and absorption was measured in electron yield mode. Theoretical spectra for Gd^{2+} and Gd^{3+} valence at the Gd $M_{5,4}$ X-ray edges were generated via atomistic multiplet calculations using code by van Veenendaal, in which the Hamiltonian includes the Coulomb interactions in the 4f shell and those between the 4f shell and the core hole and the spin−orbit coupling. Parameters were obtained in the Hartree−Fock limit using Cowan's code and the values for the Coulomb interaction were scaled down to 80% to account for screening effects, producing good agreement between theory and experiment.[56,57] These theoretical XAS spectra for Gd^{2+} and Gd^{3+} were interpolated and fit to the experimental XAS data.

Magnetic Measurements. Magnetic characterization was performed on a Quantum Design Physical Property Measurement System (PPMS - 9T) equipped with a Vibrating Sample Magnetometer (VSM). $Eu_{1-x}Gd_xS$ NC samples were stored in the glovebox after synthesis and were placed in a Teflon bucket attached to a carbon fiber rod for measurement. Zero field-cooled and field-cooled scans of magnetization as a function of temperature were performed from 5 to 300 K with an external field of 100 Oe. Hysteresis curves were collected from −9 to 9 T at low (5−6 K) and high (100 and/or 300 K) temperatures. Magnetic isotherms, where magnetization is measured as a function of field for a given temperature, were measured for a range of temperatures surrounding the T_C of EuS (16.7 K) for use in Arrott plot calculations of T_C. Diamagnetic contributions were negligible.

Results and Discussion

Synthesis and Characterization of Precursors. Thermally decomposing Eu SSPs with dithiocarbamate (dtc) ligands in hot organic solvents is the most commonly employed and arguably the most effective method for synthesizing EuS NCs.[44,47−51] Such SSPs are neutral coordination complexes of an Eu^{3+} ion with three dtc ligands, and either a phenanthroline or bipyridine ligand. When heated to ca. 300 °C in organic solvents, they decompose via an internal redox reaction, resulting in EuS NCs. Since bonds within the SSP must break during the reactions, the structure and properties of these precursors could affect their performance. We designed new precursors attempting to refine/modify the decomposition behavior of these SSPs and therefore better control the synthesis of EuS NCs. A more refined synthesis of EuS NCs provides the foundation for designing an effective method for synthesizing $Eu_{1-x}Gd_xS$ NCs. Bulk crystals and thin films of Gd doped EuS have been prepared through co-melting, electron-beam deposition, and flash evaporation (methods incompatible with all existing EuS NC synthetic schemes) and have been shown to have enhanced T_C up to 50 K.[39,41]

First, we made Eu SSPs using dtc ligands with bulkier hydrocarbon rings, such as Pytc, Pipdc, and Mpipdc (the chemical structures and abbreviations for these precursors are found in Scheme 1). Furthermore, following the most successful Eu SSPs, we designed analogous Gd dtc SSPs using Ddtc and Pytc and bipyridine ligands and synthesized them in similar aqueous reactions. The theory was that the similarity of these structures would allow for similar decomposition behavior and reactivity to facilitate the growth of mixed NCs. Prior to attempting the doping synthesis, we characterized these new SSPs (**1**−**5**) and determined the suitability of each for reproducibly growing monodisperse, crystalline NCs.

The new precursors were characterized using single-crystal X-ray crystallography. The structure refinement data for precursors **1**−**5** can be found in Table 1 and the structures are displayed in Figure 1. As seen in Table 2, despite the varied composition of the ligands, the most important bond lengths between metal and coordinating ligand atoms, and their bond angles are quite similar. Additionally, these bond lengths and angles are similar to those published for a variety of EuS dithiocarbamate NC precursors.[47]

FTIR shifts for the C−S and C−N stretches show remarkable similarity between precursors. TGA (Figure 2) showed relatively similar decomposition temperature for all the precursors (over the range of 200−350 °C); however, the slope of the decomposition curve was much steeper for some precursors than for others. It should be noted that TGA is solid-state thermal decomposition in a nitrogen atmosphere, while NCs synthesis is solution thermolysis. Therefore, even though the behavior observed in TGA is a useful indicator, it might not fully predict the behavior expected during NC synthesis.

Optimization of Precursors in the Synthesis of Pure EuS Nanocrystals. Use of SSPs allows for the synthesis of NCs from reactive or insoluble precursors (such as the Eu^{2+} salts) while providing all elements found in the final NCs in a fixed ratio. In the case of Eu dtc SSPs, the ratio is 6 S^{2-} ions for every Eu^{3+} ion. The highest quality EuS NCs in crystallinity, morphology, and dispersity have been observed from decomposition of these SSPs in high boiling point solvents such as trioctylphosphine, oleylamine, oleic acid, and octadecene. Despite the general success, synthesis of EuS NCs using SSPs still suffers from a lack of reproducibility (specifically SSP batch variation) and purity (NCs samples can contain high percentages

(55) Trebbia, P.; Bonnet, N. *Ultramicroscopy* **1990**, *34*, 165.
(56) Cowan, R. D. *J. Opt. Soc. Am.* **1968**, *58*, 808.
(57) Thole, B. T.; van der Laan, G.; Fuggle, J. C.; Sawatzky, G. A.; Karnatak, R. C.; Esteva, J.-M. *Phys. Rev. B* **1985**, *32*, 5107.

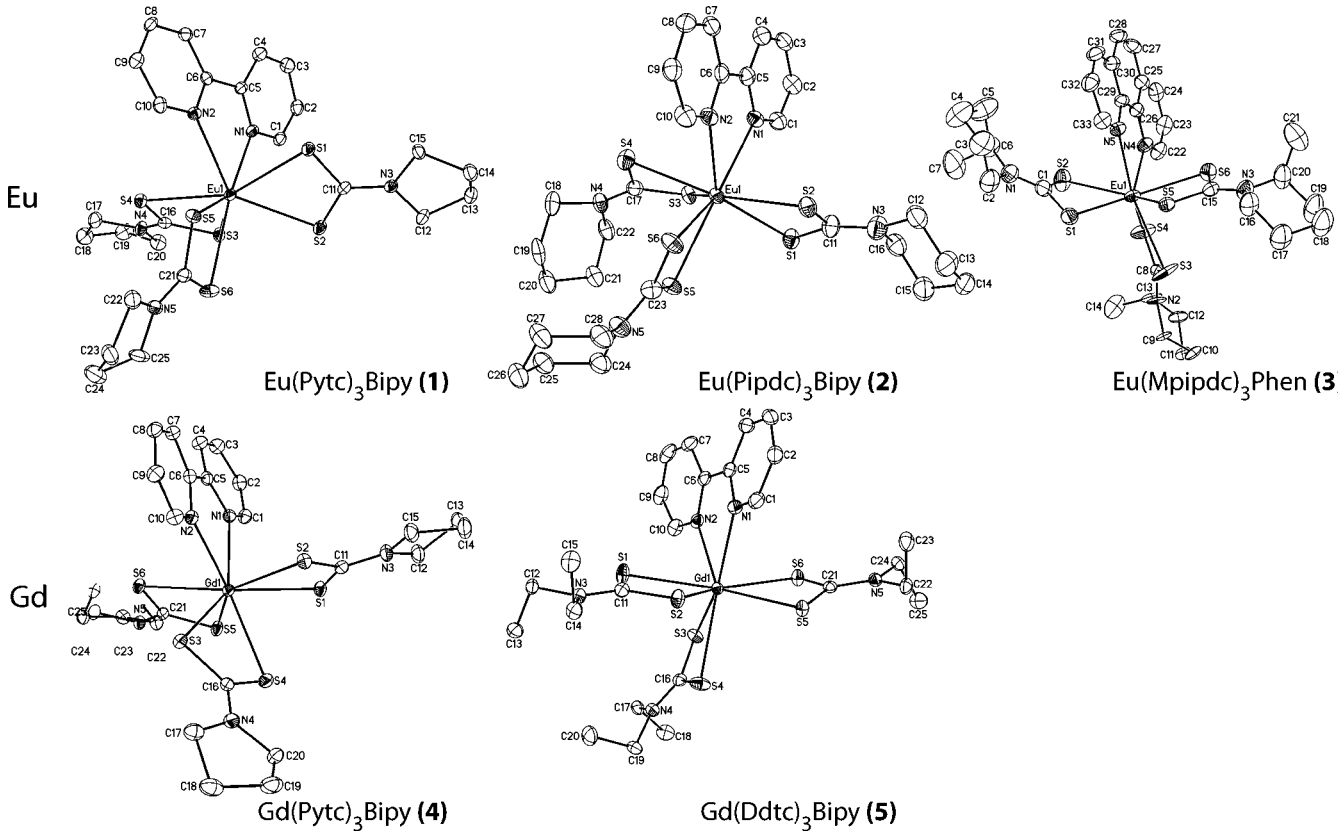

Figure 1. X-ray crystal structures for precursors **1**−**5**.

Table 2. Selected Bond Lengths and Angles in Precursors **1**−**5**

bond length (Å)	1	2	3	4	5
M(1)−N(1)	2.560(3)	2.595(5)	2.569(4)	2.5493(19)	2.573(2)
M(1)−N(2)	2.587(3)	2.642(5)	2.577(4)	2.5770(18)	2.5914(19)
M(1)−S(1)	2.8891(9)	2.8416(16)	2.8038(14)	2.8857(6)	2.7941(6)
M(1)−S(2)	2.8879(9)	2.8438(15)	2.8314(15)	2.8553(6)	2.8891(5)
M(1)−S(3)	2.8879(9)	2.8584(14)	2.984(6)	2.8360(6)	2.8918(6)
M(1)−S(4)	2.8611(9)	2.8154(15)	2.865(3)	2.8526(6)	2.8274(6)
M(1)−S(5)	2.8443(10)	2.8578(14)	2.8671(12)	2.8269(6)	2.8267(5)
M(1)−S(6)	2.8577(10)	2.8522(15)	2.8588(13)	2.8865(6)	2.8374(6)

bond angle (deg)	1	2	3	4	5
S(1)−M(1)−S(2)	62.68(3)	62.75(4)	63.35(4)	62.469(16)	62.851(16)
S(3)−M(1)−S(4)	62.34(3)	62.69(4)	60.39(13)	63.177(17)	62.167(16)
S(5)−M(1)−S(6)	62.96(3)	62.19(4)	61.84(3)	62.843(15)	63.075(15)
N(1)−M(1)−N(2)	63.85(9)	62.85(16)	64.30(13)	64.19(6)	63.34(6)

averages	1	2	3	4	5
M−N (Å)	2.573(8)	2.619(0)	2.573(4)	2.5631(7)	2.582(3)
M−S (Å)	2.8639(3)	2.8448(8)	2.868(5)	2.857(3)	2.8444(7)
C−S (Å)	1.719(1)	1.725(1)	1.727(1)	1.720(9)	1.725(0)
S−M−S (deg)	62.66(3)	62.54(7)	61.86(3)	62.829(8)	62.69(8)

of Eu^{3+} ions, likely due to amorphous coatings, despite appearing to be 100% EuS by X-ray diffraction techniques).[58]

A primary motivation for exploring new SSPs was the thought that varying the structure of the ligands on dithiocarbamate precursors could affect the decomposition behavior, that is, potentially changing the temperature of decomposition or the identity/quality/structure of the decomposition products. However, only minor variance was observed. One potential reason for this similarity in decomposition is the structural similarity of all SSPs as revealed by X-ray crystallography (Table 2). Solution-phase thermolysis was performed using all new Eu SSPs **1**−**3** plus $Eu(Ddtc)_3Bipy$ to ensure that they would form the desired EuS NCs (TEM images of representative NCs can be found in Figure S1). After extensive comparison of the results, **1** was shown, by a slight margin, to most reproducibly

(58) Selinsky, R. S.; Keavney, D. J.; Bierman, M. J.; Jin, S. *Appl. Phys. Lett.* **2009**, *95*.

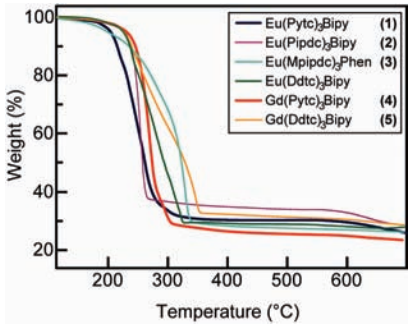

Figure 2. TGA of single source precursors **1**−**5** and $Eu(Ddtc)_3Bipy$.

yield the most monodisperse EuS NCs. **1** was used as the Eu SSP for all syntheses of doped NCs.

For the synthesis of $Eu_{1-x}Gd_xS$ NCs, we desired an Eu SSP and a Gd SSPs which would decompose simultaneously to result in homogeneous distribution of Eu and Gd within each NC. The corresponding Gd precursor **4** was chosen for being most likely to share reactivity and decomposition behavior with **1** due to their structural similarities. The assumption of simultaneous solution decomposition is partially supported by the similar thermal decomposition behaviors seen in Figure 2, where **1** and **4** decompose at 190−315 °C and 210−305 °C, respectively. For all doped $Eu_{1-x}Gd_xS$ NCs whose magnetic properties were analyzed in this paper, this pair of SSPs was used in their syntheses.

Doped (Mixed) Nanocrystal Synthesis. While there are previous reports of the synthesis of pure EuS NCs,[47−49] there have been no reports of doped EuS NCs syntheses. The first step in the synthesis of EuS NCs is to make a suspension of the Eu SSP in TOP. Similarly, the first step in the synthesis of $Eu_{1-x}Gd_xS$ NCs was to make a suspension of **1** and **4** in a desired ratio in TOP. Because of their similar decomposition behavior, when mixed suspensions of Eu and Gd SSPs are injected into a hot mixture of TOP and oleylamine at 290 °C, they decompose simultaneously resulting in the nucleation of a single alloyed phase and subsequent growth of doped NCs. It should be noted that successful uniform doping in NCs is known to be challenging due to both thermodynamic and kinetic factors;[59] therefore, simultaneous decomposition does not necessarily guarantee uniform distribution of Gd ions. However, as discussed later, extensive characterization of $Eu_{1-x}Gd_xS$ prepared via this method provided strong evidence for the fact that they have been homogenously doped.

All of the $Eu_{1-x}Gd_xS$ samples we prepared and investigated in detail are listed in Table 3. A majority of $Eu_{1-x}Gd_xS$ samples we have prepared (samples A−K) have low concentrations of Gd (≤10%) because these are ratios predicted by theory and shown in the bulk to yield the highest enhancements in T_C. The synthesis was also attempted where the SSPs were injected separately 30 min apart with no appreciable difference in physical properties or morphology of the resultant crystals as in the case for shaded samples E, G, I, M, O, P in Table 3.

Nanocrystal Structure/Composition Analysis. TEM examination (Figure 3) revealed semispherical NCs with dispersity and diameters (∼6−12 nm, average 8 nm) comparable to those reported for pure EuS NCs and relatively consistent independent of the ratio of Eu/Gd precursors used (or the ratio of Eu/Gd found in the NCs). PXRD (Figure S2) gave peaks consistent with a rock-salt crystal structure and no other crystalline phase of rare earth compound, although from previous study we know there is likely an amorphous component.[58] GdS and EuS share the same rock-salt structure and nearly the same lattice parameters (EuS is 6.7% larger).[35,36] Vegard's Law predicts the PXRD peaks should shift with increasing Gd concentration due to differing lattice constants. The PXRD peak locations are within experimental error of those predicted (Figure S2). From the PXRD peak broadening, the average NC diameter can be estimated using the Scherrer formula to be about 6.7 nm (see Supporting Information), consistent with the average diameter estimated from TEM images.[60]

Table 3. Summary of Doped Samples of $Eu_{1-x}Gd_xS$ NCs[a]

Sample	% Gd in SSP mixture	% Gd in NCs by ICP-AES	T_C (K)	θ (K)
A*	0	-	16.8	15.8
B	0	-	19.5	16.7
C*	0	-	24.1	15.2
D	1	0.3	27.0	19.1
E	5	2.6	28.9	78.6
F	5	2.9	23.3	78.0
G	5	3.7	26.1	81.5
H	10	3.9	22.6	20.9
I	5	4.3	26.6	79.7
J	5	5.3	29.4	83.2
K	10	9.0	20.2	77.6
L	20	17.7	10.9	32.2
M+	50	41.6	10.9	1.4
N+	60	46.7	-	−21.7
O+	50	50.4	4.5	0.6
P+	50	50.4	10.2	8.4
Q+	80	72.1	-	−54.4

[a] Shaded rows signify samples synthesized using multiple injections of precursors. Asterisks (*) indicate synthesized from $Eu(Ddtc)_3Phen$. Symbol (+) indicates the T_C values are approximate for samples M−Q due to deviation from parameters required for Arrott plot assumptions to be valid.

Understanding the changes to the magnetic properties requires the knowledge that Gd ions are integrated into the EuS NC lattice and with what exact amount. The ratio of Eu to Gd was confirmed by ICP-AES on digested NCs to be consistent with the ratio of Eu to Gd precursors employed for the synthesis, as tabulated in Table 3. The close correlation between the ratio of SSPs injected and the ratio of Eu to Gd found in the $Eu_{1-x}Gd_xS$ NC products demonstrates the targeted tunability of this method.

While conclusively proving true, homogeneous doping is very difficult for nanomaterial samples, from our various experimental observations we are confident in significant integration of Gd into the EuS NCs. Since ICP-AES unequivocally confirms that both Eu and Gd are contained in the samples, the fact that only one size and morphology of NCs was observed for each sample under TEM suggests that both ions are located within the same NCs.

More importantly, STEM (Figure 4) was used to confirm that Eu and Gd were uniformly distributed between NCs and within the NCs. Each EELS map presented in Figure 4 is an image composed of 2500 pixels, where each pixel contains the analysis of one EELS spectrum. The average EELS spectrum of all 2500 spectra is shown in Figure 4b with the relevant Eu and Gd edges labeled. The EELS maps of the intensities of the Eu M_5 (Figure 4c) and Gd M_5 edges (Figure 4d) clearly show that Eu and Gd are contained within the same NC (i.e., the sample is not a

(59) Erwin, S. C.; Zu, L.; Haftel, M. I.; Efros, A. L.; Kennedy, T. A.; Norris, D. J. *Nature* **2005**, *436*, 91.

(60) Denton, A. R.; Ashcroft, N. W. *Phys. Rev. A* **1991**, *43*, 3161.

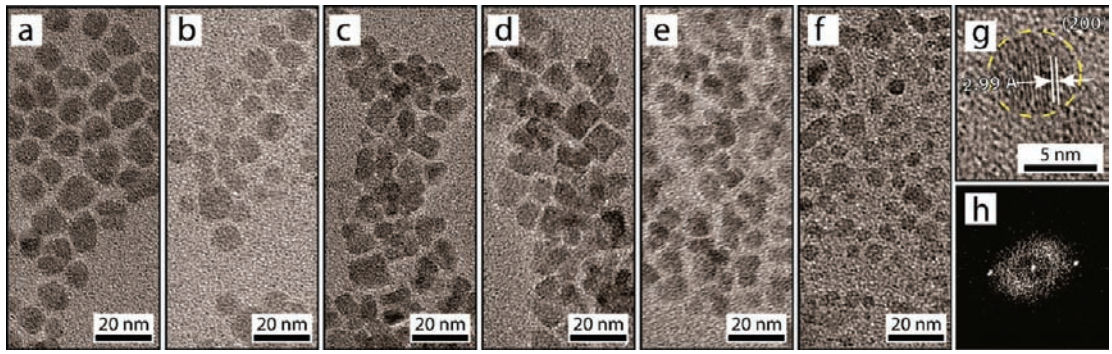

Figure 3. TEM images of doped $Eu_{1-x}Gd_xS$ NCs: (a) $x = 0.014$, (b) $x = 0.026$, (c) $x = 0.042$, (d) $x = 0.065$, (e) $x = 0.129$, (f) $x = 0.066$, (g) HRTEM for a NC from panel f, and (h) FFT of panel g.

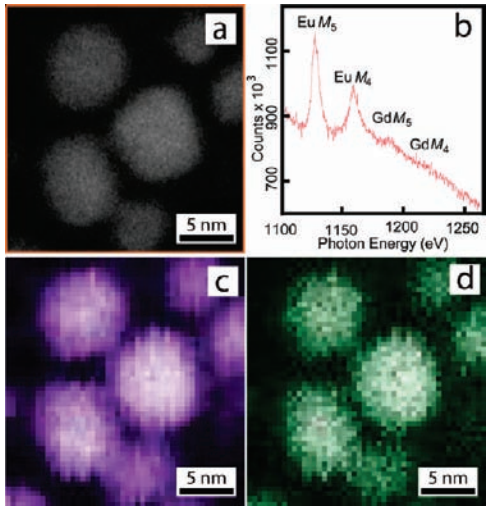

Figure 4. (a) STEM image of $Eu_{1-x}Gd_xS$ NCs ($x = 0.066$) mapped using EELS (50 × 50 spectra); (b) the average of all the EELS spectra present in the EELS map. The Eu M_5 and Gd M_5 edges used for examining elemental distribution are indicated. (c) EELS map of Eu M_5 edge intensity and (d) EELS map of Gd M_5 edge intensity.

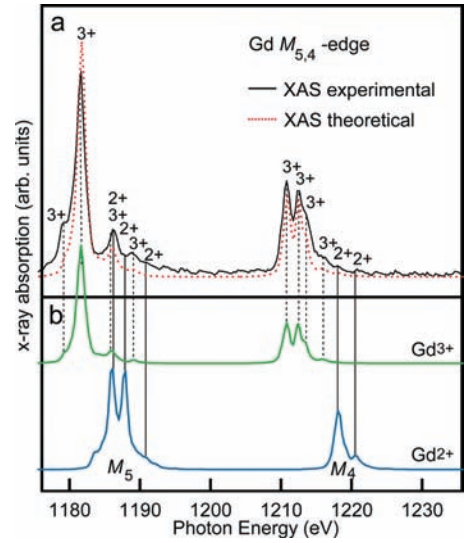

Figure 5. (a) Experimental XAS spectrum of Gd $M_{5,4}$ edges for an ensemble of $Eu_{1-x}Gd_xS$ NCs ($x = 0.066$) and measured at 8 K and the weighted sum of theoretical Gd^{2+} and Gd^{3+} XAS multiplet spectra. (b) Theoretical XAS multiplet spectra for Gd^{2+} and Gd^{3+} ions for comparison.

mixture of EuS NCs and GdS NCs) and that the two elements are uniformly distributed within each NC. While not atomically resolved, this experiment is consistent with spatially uniform distribution of Gd and Eu ions in each NC.

Additional strong support for the integration of Gd and Eu within a single NC is the enhancement in magnetic properties observed (see below). If EuS and GdS were completely segregated, one would expect the magnetic measurements to be consistent with a simple addition of the magnetic behaviors of each separate component. For example, for a 10% Gd sample, complete segregation would result in the magnetization curves composed of the sum of 90% EuS ferromagnetic character and 10% GdS antiferromagnetic character. The observed magnetic behavior cannot be explained by a mixture of separate EuS and GdS NCs.

The Electronic State of the Gd Dopants. Synchrotron XAS data of the Gd $M_{5,4}$ edges (Figure 5) was collected for a $Eu_{1-x}Gd_xS$ NC sample ($x = 0.129$). Theoretical XAS spectra for Gd^{2+} and Gd^{3+} were generated, interpolated to the experimental energy values, and a linear combination of them fit to the experimental XAS data. The best fit of this data ($R^2 = 0.89$) yields a composition of 97% Gd^{3+} and 3% Gd^{2+}. This shows the predominance of the dopant Gd^{3+} ions in the $4f^7$ spin ground state, as expected.[14,38−40]

Characterization of Magnetic Properties. Systematic physical and magnetic characterization was performed on ensembles of each $Eu_{1-x}Gd_xS$ NC sample listed in Table 3. The dependence of dopant concentration in EuS on magnetic behavior has been studied extensively in the bulk. To determine the T_C of each $Eu_{1-x}Gd_xS$ NC sample, we employed Arrott plots, a method which uses magnetic saturations extrapolated from magnetic isotherms to determine the transition temperature.[61] This technique has been used previously to determine the T_C of EuS NCs, and we followed the steps outlined by Stoll.[52] Magnetic isotherms (M^2 vs H/M) were taken for temperatures near the expected T_C and the representative magnetic isotherms for NC sample E are shown in Figure 6a. The high-field regions of the isotherms can be fit to the linear equation

$$M^2 = A(H/M) + B(T_C - T) \quad (1)$$

where M is magnetization, H is applied field, T is temperature, and $A = 1/bT$ and $B = a/bT$ (a and b are constants). The spontaneous magnetization, M_s, is defined as the magnetization of a material at zero applied field. Therefore, the intercept of each isotherm with the M^2 axis corresponds to its M_s^2 value.

(61) Arrott, A.; Noakes, J. E. *Phys. Rev. Lett.* **1967**, *19*, 786.

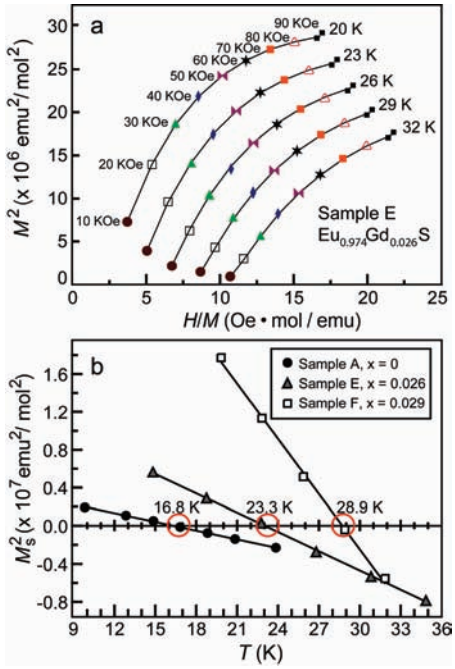

Figure 6. (a) The Arrott plot for a representative doped $Eu_{1-x}Gd_xS$ NC sample (Sample E) with a $T_C = 28.9$ K; (b) the M_s^2 vs T plots for several representative $Eu_{1-x}Gd_xS$ NC samples to determine the T_C.

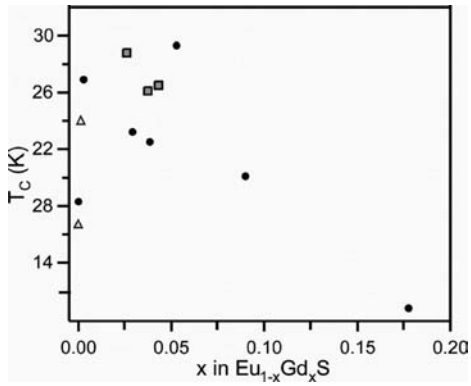

Figure 7. T_C of $Eu_{1-x}Gd_xS$ NCs vs Gd fraction for $0 \leq x \leq 0.2$. Circles represent samples prepared from single injection reactions, squares indicate multiple injection reactions of $M(Pytc)_3Bipy$ (M = Eu, Gd), and triangles indicate syntheses using $Eu(Ddtc)_3Phen$ SSP.

Thus, considering only magnetization values at zero applied field, eq 1 is reduced to

$$M_s^2 = BT_C - BT \qquad (2)$$

Each M_s^2 is plotted against the temperature of its corresponding isotherm and fitted with linear eq 2, as shown for representative NC samples A, E, and F in Figure 6b. The intercept of the M_s^2 plot with the x-axis is the temperature where $M_s^2 = 0$ and thus gives the T_C, below which spontaneous magnetization occurs.[52] This approximation is only valid for ferromagnetic samples where the magnetic isotherms are taken near the T_C. These requirements are not met for samples O to Q.

The complete collection of Gd concentrations, Curie temperatures, and Weiss constants (see later) for doped $Eu_{1-x}Gd_xS$ NCs synthesized is summarized in Table 3. Figure 7 displays the T_C as a function of Gd concentration for all ferromagnetic samples (A−L). This clearly shows the most significant T_C enhancement occurs over the range 2.6−5.3% Gd with the highest T_C at 29.4 K. This is slightly greater than the concentration regime of highest T_C enhancement reported for bulk $Eu_{1-x}Gd_xS$ (1−3% Gd).[39] The overall behavior qualitatively follows the theoretical model of the RKKY coupling mechanism where localized spins are coupled through conduction electrons.[14,38−41] Just as seen experimentally, Gd^{3+} ions provide the same local moments as Eu^{2+} and add electron density to the conduction band, which in turn improves the magnetic coupling, therefore, enhancing the T_C.[40] The added electron density also compensates for Eu^{3+} defects and S vacancies known to be present in EuS. When a small amount of Gd ions is added, the coupling between Eu^{2+} is increased. When too many electrons are added, the density is too large for only the lower energy spin state of the conduction band to be occupied and the benefit diminishes. With excess electrons, the exchange splitting of the conduction band is not sufficiently large to maintain complete spin polarization of the conduction electrons.[14,39] One possible explanation for the smaller enhancement of T_C as compared to those observed for doped bulk EuS is the size of the materials. Nanocrystals have a higher surface to volume ratio and this surface can act as defect sites trapping electron density. Additionally, reduction in overall magnetism has been reported for small, undoped EuS NCs because they are thought to be approaching their superparamagnetic limit.[26]

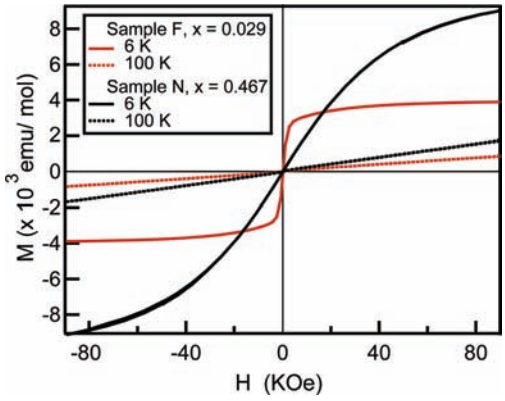

Figure 8. Representative hysteresis loops of $Eu_{1-x}Gd_xS$ NCs at temperatures above and below the magnetic transition temperatures. Sample F ($Eu_{0.970}Gd_{0.029}S$) shows ferromagnetic behavior at 6 K and paramagnetic behavior at 100 K. Sample N ($Eu_{0.533}Gd_{0.467}S$) shows antiferromagnetic behavior at 6 K and paramagnetic behavior at 100 K.

We also characterized the magnetization behavior of each $Eu_{1-x}Gd_xS$ NC sample. As shown in Figure 8, hysteresis loops (scans of magnetization as the function of external magnetic field) were taken, one below and one above the expected magnetic transition temperatures given the T_C for pure EuS of 16.6 K and a T_N for pure GdS of 59 K.[36,62,63] For doped samples containing less than or equal to 9% Gd (samples D−K), the T_C is enhanced as compared to pure EuS NCs (samples A−C). For those with greater than 9% Gd, the T_C is depressed (samples L−Q). For samples A−K, below the T_C (determined using the Arrott method discussed above), a small but measurable hysteresis is present excluding superparamagnetic behavior but indicating ferromagnetism. As the concentration of Gd increases,

(62) Bruckel, T.; Hupfeld, D.; Strempfer, J.; Caliebe, W.; Mattenberger, K.; Stunault, A.; Bernhoeft, N.; McIntyre, G. J. *Eur. Phys. J. B* **2001**, *19*, 475.
(63) Kobler, U.; Hupfeld, D.; Schnelle, W.; Mattenberger, K.; Bruckel, T. *J. Magn. Magn. Mater.* **1999**, *205*, 90.

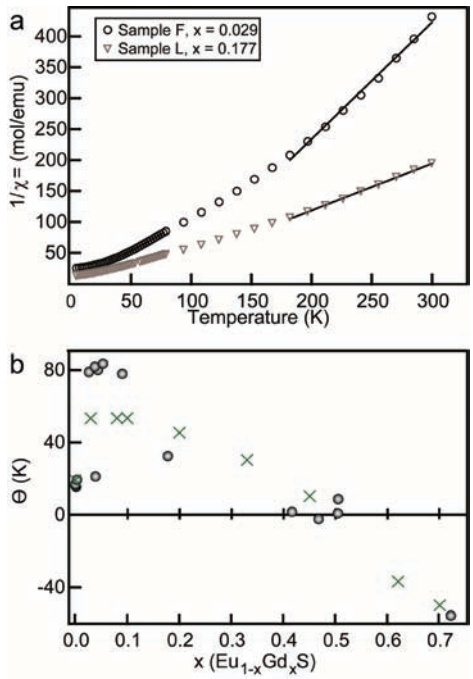

Figure 9. (a) Curie−Weiss determination of paramagnetic Curie temperature θ (temperature dependence of inverse susceptibility); (b) θ vs the Gd composition (x) of $Eu_{1-x}Gd_xS$ NCs for $0 \leq x < 0.8$, where the circles represent experimental results determined in this study and the crosses represent literature reported values for bulk doped $Eu_{1-x}Gd_xS$.[41]

the observed magnetism becomes softer. For samples L−S, below the T_C, the behavior is largely paramagnetic although it is not completely linear which suggests some saturation behavior. For all samples from A−Q, above their T_C, their behavior is paramagnetic.

Finally, we determined the Weiss constant for each NC sample using the Curie−Weiss law

$$1/\chi = (T - \theta)/C \tag{3}$$

where χ is the magnetic susceptibility, T is the temperature, C is the Curie constant, and θ is the Weiss constant. Temperature-dependent magnetic susceptibility data were taken for each sample and inverse magnetic susceptibility was plotted as a function of temperature to give a linear fit of the paramagnetic region as shown in Figure 9a.[64] The Weiss constants for all $Eu_{1-x}Gd_xS$ NC samples are listed in Table 3 and are displayed in Figure 9b for samples A−Q. Positive Weiss constant values indicate that a material is ferromagnetic and negative values indicate antiferromagnetism. As seen in Figure 9b, for samples with low Gd concentrations, the Weiss constant is both positive and enhanced as compared to undoped EuS, consistent with bulk values[41] where the literature values are represented by crosses and our experimental values are represented by circles. As the concentration of Gd increases, the Weiss constant decreases, eventually becoming negative indicating the transition to antiferromagnetism.[39,65−67] The trend and values for the $Eu_{1-x}Gd_xS$ NC samples are similar to those published for bulk samples.[41]

Conclusion

In conclusion, enhancement of the Curie temperatures and other modifications of magnetic properties of EuS NCs have been shown through doping with Gd. New EuS and GdS single source precursors were synthesized and characterized, then explored to facilitate their use in the synthesis of mixed (doped) $Eu_{1-x}Gd_xS$ NCs with a variety of relative ratios of Gd to Eu. Those ratios were quantitatively measured using ICP-AES and the uniformity of the dopant distribution confirmed by EELS mapping with STEM. A systematic investigation of magnetic properties showed the doping concentration of Gd directly influences the T_C, θ, and hysteretic behavior of the $Eu_{1-x}Gd_xS$ NCs. The T_C is dependent on the Gd concentration with a peak T_C of 29.4 K for a sample containing 5.3% Gd. The trends in magnetic behavior are qualitatively comparable to those observed for bulk Gd doped EuS samples. To fully understand the contributions from Gd and Eu to the observed magnetism, these $Eu_{1-x}Gd_xS$ NC samples will be further investigated using X-ray magnetic circular dichroism (XMCD) techniques[58] in the future.

Acknowledgment. This work is supported by NSF (DMR-0548232) and NIH (CA126701). S.J. also thanks Research Corporation Cottrell Scholar award, Sloan Research Fellowship, ExxonMobil Solid State Chemistry Fellowship, and Dupont Young Professor Grant for support. As an REU student at UW-Madison, E.A.M.P. was supported by the UW-Madison Nanoscale Science and Engineering Center, UW-Madison Department of Chemistry, UW-Madison Graduate School, and University of Puerto Rico-Cayey RISE program. We would like to thank Prof. Paul Voyles for his help in EELS analysis, Dr. Alexander Kvit for his assistance gathering STEM data, Dr. David Keavney for his help gathering XAS data and his ongoing assistance, and Dr. Michel van Veenendaal for his assistance with atomistic multiplet calculations. Use of the Advance Photon Source was supported by the U.S. Department of Energy, Office of Science, Office of Basic Energy Sciences, under Contract DE- AC02-06CH11357.

Supporting Information Available: TEM images of EuS NCs synthesized with alternative SSPs, PXRD of $Eu_{1-x}Gd_xS$ NCs and associated analysis, X-ray crystallographic files (CIF) and tables of crystal data, structure solution and refinement, atomic coordinates, and bond lengths and angles for the precursors listed in Table 1. This material is available free of charge via the Internet at http://pubs.acs.org.

JA104314C

(64) Kittel, C. *Introduction to Solid State Physics*, Seventh ed.; John Wiley & Sons: New York, Chichester, 1996.
(65) Bayer, E.; Zinn, W. Z. *Angew. Phys.* **1971**, *32*, 83.
(66) McGuire, T. R.; Holtzber, F.; Moruzzi, V. L. *Bull. Am. Phys. Soc.* **1971**, *16*, 326.
(67) Methfessel, S.; Holtzberg, F.; McGuire, T. R. *IEEE Trans. Magn.* **1966**, *MAG2*, 305.